# Production of $\phi$ Mesons in Near-Threshold $\pi N$ and $N N$ Reactions

A.I. Titov $^{a,b*}$, B. Kämpfer $^{a\dagger}$ and B.L. Reznik $^{c\ddagger}$,

$^a$ *Forschungszentrum Rossendorf, PF 510119, 01314 Dresden, Germany*

$^b$ *Bogoliubov Laboratory of Theoretical Physics, JINR, Dubna 141980, Russia*

$^c$ *Far-Eastern State University, Sukhanova 9, Vladivostok 690090, Russia*

## Abstract

We analyze the production of $\phi$ mesons in $\pi N$ and $N N$ reactions in the near-threshold region, using throughout the conventional "non-strange" dynamics based on such processes which are allowed by the non-ideal $\omega - \phi$ mixing. We show that the occurrence of the direct $\phi N N$ interaction may show up in different unpolarized and polarization observables in $\pi N \to N \phi$ reactions. We find a strong non-trivial difference between observables in the reactions $pp \to pp\phi$ and $pn \to pn\phi$ caused by the different role of the spin singlet and triplet states in the entrance channel. A series of predictions for the experimental study of this effect is presented.

key words: hadron reactions, phi production, threshold
PACS number(s): 13.75.-n, 14.20.-c, 21.45.+v

Typeset using REVTEX

$^*$E-mail address : `atitov@thsun1.jinr.ru`

$^\dagger$E-mail address : `kaempfer@fz-rossendorf.de`

$^\ddagger$E-mail address : `reznik@dvgu.ru`

# I. INTRODUCTION

The present interest in the $\phi$ meson production in different elementary reactions is related to the strangeness degrees of freedom in the nucleon. Since the $\phi$ meson is thought to consist mainly of strange quarks, i.e. $s\bar{s}$, with a rather small contribution of the light $u$ and $d$ quarks, its production should be suppressed if the entrance channel does not possess a considerable admixture of strangeness. Indeed, the recent experiments on the proton annihilation at rest (cf. [1] for references and a compilation of data) point to a large apparent violation of the OZI rule [2], which is interpreted [1] as a hint to an intrinsic $s\bar{s}$ component in the proton. However, the data can be explained as well by modified meson exchange models [3] without introducing any strangeness component in the nucleon or OZI violation mechanisms. On the other hand, the analysis of the $\pi N$ sigma term [4] suggests that the proton might contain a strange quark admixture as large as 20%. Thus this issue remains controversial. Therefore it is tempting to look for other observables [1,5,6] that are sensitive to the strangeness content of the nucleon. Most of them are related to a possible strong interference of delicate $s\bar{s}$ knock-out and shake-off amplitudes and the "non-strange" amplitude which is caused by OZI rule allowed processes, or by processes wherein the standard OZI rule violation comes from the $\phi - \omega$ mixing.

As shown in Ref. [6], through this interference the polarization observables of the $\phi$ *photoproduction* process are sensitive even to a rather small strangeness admixture in the proton. However, the only $^{3,1}S$ $s\bar{s}$ configurations may be seen in a such process. The other configurations, such as $^{3,1}P$, are suppressed by the selection rules and/or form factors. Contrary to this, Ellis et al. [7] argue that the possibly dominant $^3P_1$ configuration might be seen in *hadronic* reactions.

Obviously, reliable information about the hidden strangeness manifestation in the $\phi$ production in $\pi p$ and $NN$ reactions can be obtained only when the conventional, i.e. non-exotic, amplitude has been understood quantitatively. This is the objective of this work. The dominant conventional processes in $\pi N$ and $NN$ reactions are depicted in Figs. 1 and 2,

where (a) is the mesonic exchange process being allowed by the finite $\phi\rho\pi$ coupling strength and (b) is the direct $\phi$ radiation from the nucleon legs, which is proportional to the finite $\phi NN$ interaction strength. It should be emphasized that the process 1a is a subprocess in the diagram 2a, while the process 1b is a subprocess in the diagram 2b, when the exchanged boson is a pion.

While the diagrams in Figs. 1 and 2 look like usual Feynman diagrams it should be stressed they give a guidance of how to obtain from an interaction Lagrangian of hadronic fields a covariant parameterization of observable in strict tree level approximation. Additional ingredients are needed to achieve an accurate description of data within such a framework. In particular, the vertices needs to be dressed by form factors.

The early theoretical studies [8,9] show, indeed, that predictions for hadronic observables are very sensitive to the parameters of the monopole form factors which can not be fixed unambiguously without adjustments relying on the corresponding experimental data. In our case one can rely on the recent measurement of the ratio of the total cross sections of $\phi$ and $\omega$ production in $pp$ reactions studied by the DISTO Collaboration at SATURNE at $T_{\text{lab}} = 2.85$ GeV as well as on the $\phi$ angular distribution in the $pp \to pp\phi$ reaction [10] and on the total cross section [11].

In the (sub)threshold region also in heavy-ion reactions the $\phi$ production data is accessible via the $K^+K^-$ decay channel studied with the $4\pi$ detector FOPI at SIS in GSI/Darmstadt [12]. However, here an understanding of elementary hadronic reactions serves as a prerequisite for interpreting the data. Rather the upcoming proton and pion beam experiments with the HADES detector system at SIS in GSI [13] offer a chance to enlarge the data base. In particular, HADES can identify the $\phi$ also via the $e^+e^-$ channel.

Finally we mention that for pion-induced reactions at the proton also near-threshold data for the $\phi$ production are available [14].

An important step towards an understanding of the structure of the "non-strange" $pp \to pp\phi$ reaction mechanisms was made recently [15]. The focus of Ref. [15] is the determination of the parameters of the direct $\phi NN$ interaction, thus reducing the above mentioned

3

uncertainties, by analyzing the combined the $pp \to pp\omega$ and $pp \to pp\phi$ reactions and the corresponding DISTO data [10] at a given beam energy; for the reaction $pp \to pp\omega$ just the same mechanism is assumed as those for $pp \to pp\phi$, as shown in Fig. 2. Clearly, at one given beam energies the excess energy for both reactions are quite different.

In this paper we therefore attempt a different approach with a similar goal. We reduce the uncertainties of the reaction mechanism by a combined study of the to each other related reactions $pp \to pp\phi$ and $\pi^- p \to n\phi$ using the known data within the same interval of excess energies of $20 - 100$ MeV [11,14]. For the absolute normalization of the angular distribution in $pp \to pp\phi$ [10] we use the recently published total cross sections of the reaction $pp \to pp\phi$ [11]. It turns out that this value is compatible, within given error bars, with an extrapolation of the previously measured ratio of the total cross sections of $pp \to pp\phi$ to $pp \to pp\phi$ reactions, $\sigma_\phi/\sigma_\omega = (3.7 \pm 0.5) \times 10^{-3}$ at $T_{lab} = 2.85$ GeV [10], by normalizing it to the old bubble chamber data for $\sigma_\omega$ at various excess energies [16]. The extrapolated value of the cross section differs from the new value [11] thus influencing to some extent adjusted parameters.

In comparison with previous works we are doing the next step towards an understanding of the dynamics of $\phi$ production in hadronic reactions. We present a systematical analysis of $\pi^- p \to n\phi$, $pp \to pp\phi$ and $pn \to pn\phi$ reactions in the near-threshold region where the destructive interferences between the two mechanisms (a) and (b) in Figs. 1 and 2 are essential. We are going to show that basically there are two different sets of the model parameters. One of them corresponds to the case when the mesonic exchange channel (a) is dominant for the $\pi^- p \to n\phi$ reaction (Fig. 1), and in the second case the direct emission mechanism (b) is dominant. For both sets of solutions we calculate the total and differential cross sections and spin density matrix, responsible for the $\phi \to e^+ e^-$ and $\phi \to K^+ K^-$ decay angular distributions and show in which observables the direct $\phi NN$ interaction might be clearly manifest. We present also a combined analysis of $pp \to pp\phi$ and $pn \to pn\phi$ reactions at a finite energy excess with taking into account the final state interaction and analyze the deviation of predicted observables from the pure threshold values which is important for the

future understanding of the role of an internal strangeness degrees of freedom in the nucleon. For this aim we study the beam-target spin asymmetry and the relative role of the singlet and triplet states in the entrance channel.

Our paper is organized as follows. In Section II, we define the kinematical variables and formulae for calculating the cross sections and polarization observables. The basic amplitudes for the mechanisms illustrated in Figs. 1 and 2 are given explicitly in Section III. In Section IV we discuss results of numerical calculations and predictions. The summary is given in Section V. In the Appendix we describe the formalism for the enhancement factors of final state interaction within the framework of the Jost function and the effective phase-equivalent potentials.

## II. OBSERVABLES

The differential cross section of the reaction $\pi^- p \to \phi n$ (cf. Fig. 1) has the obvious form

$$\frac{d\sigma}{d\Omega_\phi} = \frac{1}{64\pi^2 s} \frac{|\mathbf{q}|}{|\mathbf{p}_\pi|} \overline{|T_{(1)}|^2}, \tag{1}$$

where $p_\pi = (E_\pi, \mathbf{p}_\pi)$ and $q = (E_\phi, \mathbf{q})$ are the four-momenta of the pion and the $\phi$ meson in the center of mass system (c.m.s.); $\overline{|T_{(1)}|^2}$ means average and sum over the initial and final spin states, respectively.

The differential cross section of $\phi$ production in the reaction $a + b \to c + d + \phi$, where $a, b$ and $c, d$ label the incoming and outgoing nucleons (cf. Fig. 2), is related to the invariant amplitude $T_{(2)}$ as

$$d\sigma = \frac{1}{2(2\pi)^5 \sqrt{s(s - 4M_N^2)}} \overline{|T_{(2)}|^2} \frac{d\mathbf{p}_c}{2E_c} \frac{d\mathbf{p}_d}{2E_d} \frac{d\mathbf{q}}{2E_\phi} \delta^{(4)}(P_i - P_f). \tag{2}$$

where $p_n = (E_n, \mathbf{p}_n)$ with $n = a, b, c, d$ are the four-momenta of the nucleons in the c.m.s., $\sqrt{s} = E_a + E_b$ is the total c.m.s. energy, $P_{i,f}$ are the total four-momenta of the initial or final states. Hereafter $\theta$ denotes the polar $\phi$ meson angle and $\Omega$ is its solid angle. We use a coordinate system with $\mathbf{z} \parallel \mathbf{p}_a$, $\mathbf{y} \parallel \mathbf{p}_a \times \mathbf{q}$. Among the five independent variables

for describing the final state we choose $E_\phi$, $\Omega$ and $\Omega_c$. Then the energy $E_c$ of particle $c$ is defined by $E_c = \frac{AB - C\sqrt{B^2 - M_N^2(A^2 - C^2)}}{A^2 - C^2}$, with $A = 2(\sqrt{s} - E_\phi)$, $B = s - 2E_\phi\sqrt{s} + M_\phi^2$, $C = 2|\mathbf{q}|\cos\theta_{qp_c}$, Finally, the fivefold differential cross section reads

$$\frac{d^5\sigma}{dE_\phi d\Omega d\Omega_c} = \frac{1}{8(2\pi)^5\sqrt{s(s - 4M_N^2)}}\overline{|T_{(2)}|^2}\frac{|\mathbf{q}|\,|\mathbf{p}_c|^2}{|A\,|\mathbf{p}_c| + CE_c|}. \tag{3}$$

The total and/or partially differential cross sections are found by integration over the available phase space.

In this paper we consider two polarization observables. One of them is the spin density matrix which describes the spin structure of the outgoing $\phi$ meson,

$$\rho_{rr'} = \frac{\sum_\beta T_{r,\beta} T_{r',\beta}^*}{\sum_{r,\beta} T_{r,\beta} T_{r,\beta}^*}, \tag{4}$$

where $r \equiv m_\phi = \pm 1, 0$ are the spin projections of the $\phi$ meson, and $\beta$ denotes a set of unobserved quantum numbers. The spin density defines the angular distribution in $\phi \to e^+e^-$ and $\phi \to K^+K^-$ decays, which has a simple form in a system where the $\phi$ meson is at rest (for details see [9]). The decay angles $\Theta$, $\Phi$ are defined as polar and azimuthal angles of the direction of flight of one of the decay particles in the $\phi$ meson's rest frame. The decay distributions integrated over the azimuthal angle $\Phi$, $\mathcal{W}(\cos\Theta)$, depend only on the diagonal matrix elements $\rho_{00}$, $\rho_{11} = \rho_{-1-1}$, normalized as $\rho_{00} + 2\rho_{11} = 1$, according to

$$\mathcal{W}(\cos\Theta) = \frac{3}{2(B + 3)}\left(1 + B\cos^2\Theta\right), \tag{5}$$

where the $\phi$ decay anisotropies $B$ read

$$B^{K^+K^-} = -\frac{1 - 3\rho_{00}}{1 - \rho_{00}}, \quad B^{e^+e^-} = \frac{1 - 3\rho_{00}}{1 + \rho_{00}}. \tag{6}$$

To exclude the kinematical dependence of $\rho_{00}$ or $B$ on the $\phi$ meson production angle, we choose the quantization axis along the $\mathbf{z}$ direction (in the $\phi$ rest system), and using the corresponding Wigner rotation functions $d^{\cdots}_{\cdots}(\chi)$ one gets the amplitudes $T_{r,\beta}$ in Eq. (4) by

$$T^z_{m_\phi,\beta} = \sum_{\lambda,\beta'_i} T^{c.m.s.}_{\lambda,\beta'} d^1_{\lambda,m_\phi}(\chi_\phi)\prod_i d^{\frac{1}{2}}_{\beta'_i,\beta_i}(\chi_i), \tag{7}$$

6

where only $\chi_\phi = -\theta$ is important, while the other $\chi_i$'s disappear in Eq. (4).

Another polarization observable is the beam-target asymmetry in the $NN \to NN\phi$ reactions which is related to the nucleon spin states via

$$C_{BT} = \frac{d\sigma(S_i = 1) - d\sigma(S_i = 0)}{d\sigma(S_i = 1) + d\sigma(S_i = 0)}, \tag{8}$$

where $S_i$ is the total spin in the entrance channel. It is important to note that spin and parity conservation arguments result in a precise model independent prediction [17] for the beam - target asymmetry: $C_{BT} = 1$ for the $pp \to pp\phi$ reaction at the threshold. In the $pn \to pn\phi$ reaction the asymmetry depends on the relative weights of the triplet and singlet states in the entrance channel.

## III. BASIC AMPLITUDES

Basically, our consideration in this section is similar to the previous study [8] (for the pure mesonic exchange contributions depicted in Figs. 1a and 2a) and to the models [9,15] for both channels shown in Figs. 1 and 2. The difference between this work and previous ones is in the different form of cut-off form factors for the off-shell nucleons in direct $\phi$ emission (cf. Figs. 1b and 2b) and a different choice of the cut-off parameters in $\pi N$ and $NN$ interactions which we will discuss below in detail. In spite of the mentioned similarity, for completeness in discussing our predictions for the set of observables which have not been considered before, in this section we display the main formulae which define the basic amplitudes. The meson - nucleon and the $\phi\rho\pi$ interaction Lagrangians read in standard notation

$$\begin{aligned}
\mathcal{L}_{MNN} = {}&-ig_{\pi NN}\bar{N}\gamma_5\boldsymbol{\tau}\boldsymbol{\pi}N \\
&-g_{\rho NN}\left(\bar{N}\gamma_\mu\boldsymbol{\tau}N\boldsymbol{\rho}^\mu - \frac{\kappa_\rho}{2M_N}\bar{N}\sigma^{\mu\nu}\boldsymbol{\tau}N\partial_\nu\boldsymbol{\rho}_\mu\right) \\
&-g_{\phi NN}\left(\bar{N}\gamma_\mu N\phi^\mu - \frac{\kappa_\phi}{2M_N}\bar{N}\sigma^{\mu\nu}N\partial_\nu\rho_\mu\right),
\end{aligned} \tag{9}$$

$$\mathcal{L}_{\phi\rho\pi} = g_{\phi\rho\pi}\,\epsilon^{\mu\nu\alpha\beta}\,\partial_\mu\phi_\nu\,\mathrm{Tr}(\partial_\alpha\rho_\beta\pi), \tag{10}$$

where $\text{Tr}(\rho\pi) = \rho^0\pi^0 + \rho^+\pi^- + \rho^-\pi^+$, and bold face letters denote isovectors. All coupling constants with off-shell meson are dressed by monopole form factors [18] $F_i = (\Lambda_i^2 - m_i^2)/(\Lambda_i^2 - k_i^2)$, where $k_i$ is the four-momentum of the exchanged meson. Following the scheme of the meson photoproduction [19] we assume that $\phi NN$ vertices must be dressed by form factors for off-shell virtual nucleons. But this might result in a violation of the transversality of the amplitude with respect to the $\phi$ meson field. To avoid this problem we use the prescription of Ref. [19] and parameterize the product of the two form factors appearing in the left and the right diagrams in Figs. 1b and 2b in a symmetrical form

$$F_N(p_l, p_r) = \frac{1}{2}\left(\frac{\Lambda_N^4}{\Lambda_N^4 + (p_l^2 - M_N)^2} + \frac{\Lambda_N^4}{\Lambda_N^4 + (p_r^2 - M_N)^2}\right); \tag{11}$$

here $p_l$ ($p_r$) is the four-momentum of the virtual nucleon in the left (right) diagrams in Figs. 1b and 2b.

## A. $\pi N \to N\phi$ reaction

The invariant amplitude for the meson exchange channel (a) in Fig. 1 reads

$$T_{(1a)\,\lambda} = K^{\pi N} \, \epsilon^{ijkl} \left[\bar{u}(p_c)\, \Gamma_{\rho\,l}(k_\rho)u(p_a)\right] q_i k_k \, \varepsilon_j^{*\,\lambda}\, I_\pi, \tag{12}$$

where

$$\Gamma_\rho^i(k) = \gamma^i + i\frac{\kappa_\rho}{2M_N}\sigma^{ij} k_{\rho\,j}, \tag{13}$$

$$K^{\pi N}(k_\rho) = -\frac{g_{\rho NN}\, g_{\phi\rho\pi}}{k_\rho^2 - m_\rho^2}\frac{\Lambda_{\rho NN}^2 - m_\rho^2}{\Lambda_{\rho NN}^2 - k_\rho^2}\frac{\Lambda_{\phi\rho\pi}^{\rho\,2} - m_\rho^2}{\Lambda_{\phi\rho\pi}^{\rho2} - k_\rho^2} \tag{14}$$

with $k_\rho = p_c - p_a$ as the virtual $\rho$ meson's four-momentum; $\varepsilon_j^\lambda$ is the $\phi$ meson polarization vector, $I_\pi$ denotes the isospin factor being equal to $\sqrt{2}$ (1) for a $\pi^-$ ($\pi^0$) meson in the entrance channel, and the nucleon spin indices are not displayed; $i, j \cdots$ are Lorentz indices, and $\gamma_i$ and $u$ denote Dirac matrices and bispinors.

The invariant amplitude for the direct radiation channel (b) in Fig. 1 has the following form

$$T_{(1b)\,\lambda} = i g_{\phi NN} \, g_{\pi NN} \, \bar{u}(p_c) \left[ \Gamma^i_\phi(-q) \frac{\not{p}_l + M_N}{p_l^2 - M_N^2} + \frac{\not{p}_r + M_N}{p_r^2 - M_N^2} \Gamma^i_\phi(-q) \right] \bar{u}(p_c) \, \varepsilon_i^{*\,\lambda} \, I_\pi \, F_N(p_l, p_r), \quad (15)$$

where $\Gamma^i_\phi(q)$ and $F_N$ are defined by Eqs. (13) and (11), respectively, and $p_l = p_a - q$ and $p_r = p_c - q$.

## B. $NN \to NN\phi$ reaction

The total invariant amplitude of meson exchange diagrams (a) in Fig. 2 with internal meson conversion is the sum of 4 amplitudes

$$(T_M)_\alpha = \xi^1_\alpha T_M[ab; cd] + \xi^2_\alpha T_M[ab; dc] + \xi^3_\alpha T_M[ba; dc] + \xi^4_\alpha T_M[ba; cd] \qquad (16)$$

with $\xi^1_{pp} = \xi^3_{pp} = -\xi^2_{pp} = -\xi^4_{pp} = 1$, $\xi^1_{pn} = \xi^3_{pn} = -1$, $\xi^2_{pn} = \xi^4_{pn} = -2$. The last two terms stem from the antisymmetrization or from charged meson exchange in $pp$ or $pn$ reactions, respectively[1]. The first term in Eq. (16) for the $pp$ reaction reads

$$T_{(2a)\,\lambda}[ab; cd] = K^{NN} \left[ \bar{u}(p_d) \, \gamma_5 \, u(p_b) \right] \left[ \bar{u}(p_c) \, \Gamma^j_\rho(k) u(p_a) \, \epsilon_{ijkl} k^i_\rho \, q^k_\phi \varepsilon^{*\,l}_\lambda \right], \qquad (17)$$

with

$$K^{NN}(k_\pi^2, k_\rho^2) = -\frac{g_{\pi NN} \, g_{\rho NN} \, g_{\phi\rho\pi}}{(k_\pi^2 - m_\pi^2)(k_\rho^2 - m_\rho^2)} \frac{\Lambda_\pi^2 - m_\pi^2}{\Lambda_\pi^2 - k_\pi^2} \frac{\Lambda_\rho^2 - m_\rho^2}{\Lambda_\rho^2 - k_\rho^2} \frac{\Lambda_{\phi\rho\pi}^{\rho\,2} - m_\rho^2}{\Lambda_{\phi\rho\pi}^{\rho\,2} - k_\rho^2} \frac{\Lambda_{\phi\rho\pi}^{\pi\,2} - m_\pi^2}{\Lambda_{\phi\rho\pi}^{\pi\,2} - k_\pi^2}. \qquad (18)$$

The amplitude of direct $\phi$ meson emission from the nucleon legs according to Fig. 2b is calculated similarly to the real or virtual photon bremsstrahlung [20,21] in the few GeV region. The internal zig-zag lines in Fig. 2b correspond to a suitably parameterized $NN$ interaction in terms of an effective two-body $T$-matrix which is written in the form of the one-boson exchange model (OBE) with effective coupling constants and cut-off parameters and may be interpreted as effective $\pi, \omega, \rho, \sigma$ meson exchanges. We would like to stress

---

[1]In [9] we used a convention with $\xi^2_{pn} = \xi^4_{pn} = 2$, which, however, does not change our threshold prediction for the ratio of the total cross sections in $pn$ and $pp$ interaction made there without the final state interactions.

that this is an effective dynamical model which is appropriate in the few GeV region and which is different from the OBE model in the conventional sense. This model has been applied successfully to different reactions [20–22] and this encourages us to employ it for the $\phi$ production too.

The total amplitude for the process (b) in Fig. 2 consists of $2\cdot 8$ $(2\cdot 6)$ contributions for $pp$ $(pn)$ interactions and has a similar structure as Eq. (16) (with $\xi_{pn}^1 = \xi_{pn}^3 = 1$, $\xi_{pn}^2 = \xi_{pn}^4 = 0$, for $\sigma, \omega$ exchanges), where $T[ab; cd]$ now reads

$$T_{(2b)\,\lambda}[ab; cd] = -g_{\phi NN}\,\varepsilon_i^{*\,\lambda}\,[\bar{u}(p_d)V^m u(p_b)] \times$$
$$\sum_{m=\pi,\sigma,\rho,\omega} [-i\,D^m]\,\bar{u}(p_c)\left[V^m \frac{\not{p}_l + M_N}{p_l^2 - M_N^2}\Gamma_\phi^i(-q) + \Gamma_\phi^i(-q)\frac{\not{p}_r + M_N}{p_r^2 - M_N^2}V^m\right] u(p_a). \tag{19}$$

Here, $V^m$ and $D^m$ are effective coupling vertices and propagators of the two-body $T$ matrix, respectively,

$$D^{\pi,\sigma} = \frac{i}{k^2 - m_{\pi,\sigma}^2}, \quad D_{\mu\nu}^{\rho,\omega} = -i\frac{g_{\mu\nu} - k_\mu k_\nu m_{\rho,\omega}^{-2}}{k^2 - m_{\rho,\omega}^2}, \tag{20}$$

$$V^\pi = -iG_{\pi NN}\gamma_5, \quad V^\sigma = G_{\sigma NN}, \quad V_{\rho,\omega}^i(k) = -G_{\rho,\omega NN}\,\Gamma_{\rho,\omega}^i, \tag{21}$$

where $k$ is the four momentum of the virtual meson $m$ and $G_{mNN}$ is the vertex function which includes the corresponding cut-off form factor. The numerical values of the $G_{mNN}$ are taken from Refs. [20,22].

In the near-threshold region the relative velocity of the outgoing nucleons is small which might result in a strong final state interaction (FSI) between them. If the energy excess is a few MeV up to a few tens MeV then one can consider only the $s$-wave interaction and account for the final state interaction in terms of the enhancement factors by renormalizing the basic amplitude correspondingly. For instance, for the $pn$ reaction we get

$$T_{pn}[ab; cd] \rightarrow T_{pn}[ab; cd]\left(\mathcal{I}_{0pn}\,\delta_{-m_c m_d} + \mathcal{I}_{1pn}\,\delta_{m_c m_d}\right), \tag{22}$$

where $m_c, m_d$ are the spin projections of the nucleons in the final state, and $\mathcal{I}_0$, $\mathcal{I}_1$ are the singlet and triplet enhancement FSI factors, which are calculated within the Jost function

and the phase-equivalent potentials formalism, which we describe in detail in Appendix A. The calculation shows that the singlet enhancement factor is much greater than the triplet one, i.e. $|\mathcal{I}_0|^2 - 1 \gg |\mathcal{I}_1|^2 - 1 \simeq 0$ and greater than the corresponding factors of higher partial waves. Thus, for the $pp$ interaction we use

$$T_{pp}[ab; cd] \rightarrow T_{pp}[ab; cd] \left( \mathcal{I}_{0pp}\, \delta_{-m_c m_d} + \delta_{m_c m_d} \right), \tag{23}$$

reminding that at the threshold the $pp$ triplet final state is exactly zero. $\mathcal{I}_{0pn}$ and $\mathcal{I}_{0pp}$ are different which reflects the difference in the corresponding effective radii and the scattering lengths. Note that the mutual FSI of the $\phi$ and the outgoing nucleons is assumed to be negligible.

In calculating the cross sections and the spin density matrix, squares and bilinear forms of the FSI-corrected amplitudes need to be evaluated numerically.

## IV. RESULTS

### A. Fixing parameters

The parameters of the two-body $T$ matrix for the direct $\phi$ emission depicted in Fig. 2b are taken from Refs. [20,22], where a quite reasonable agreement with data of different elastic and inelastic $NN$ reactions is found.

The coupling constant $g_{\phi\rho\pi}$ is determined by the $\phi \rightarrow \rho\pi$ decay. The recent value $\Gamma(\phi \rightarrow \rho\pi) = 0.69$ MeV results in $|g_{\phi\rho\pi}| = 1.10$ GeV$^{-1}$. The SU(3) symmetry consideration [15,23] predicts a negative value for it. Thus, $g_{\phi\rho\pi} = -1.10$ GeV$^{-1}$.

The remaining parameters of the meson exchange amplitudes for the processes in Figs. 1a and 1b are taken from the Bonn model as listed in Table B.1 (Model II) of Ref. [18].

The yet undetermined parameters are: the cut-off parameters for the virtual mesons in the $\phi\rho\pi$ vertex, $\Lambda_{\phi\rho}^\pi$ and $\Lambda_{\phi\rho}^\rho$, the cut-off $\Lambda_N$ in Eq. (11), and the parameters of the $\phi NN$ interaction, $g_{\phi NN}$ and $\kappa_\phi$. We can reduce the number of parameters by making the natural assumption $\Lambda_{\phi\rho}^\pi = \Lambda_{\phi\rho}^\rho$ based on the symmetry of the virtual mesons in the $\phi\rho\pi$ vertex [15].

The next consideration is related to the tensor coupling $\kappa_\phi$. Based on the $\phi - \omega$ similarity we do not expect a large value for it and in all our subsequent calculations we employ the theoretical estimate [24] $\kappa_\phi = 0.2$ as an upper limit.

Even after that we have three free parameters being $g_{\phi NN}$, $\Lambda^\rho_{\phi\rho}$ and $\Lambda_N$. For $g_{\phi NN}$ the SU(3) symmetry predicts [25]

$$g_{\phi NN} = -\mathrm{tg}\, \Delta\theta_V\, g_{\omega NN}, \tag{24}$$

where $\Delta\theta_V$ is the deviation from the ideal $\omega - \phi$ mixing angle. It is responsible for the "standard" OZI rule violation, and in general, it depends on the method of its determination (Gell-Mann–Okubo linear or quadratic mass formulae, radiative decays, say $\phi(\omega) \to \gamma\pi$, etc.). Using the quadratic Gell-Mann–Okubo mass formula one gets $\Delta\theta_V = 3.7^0$. Sometimes another relation is used, e.g.

$$g_{\phi NN} = -3\sin\,\Delta\theta_V\, g_{\rho NN}, \tag{25}$$

which is obtained from the SU(3) relation [25]

$$g_{\omega NN} = \frac{3F - D}{F + D}\cos\Delta\theta_V\, g_{\rho NN}, \tag{26}$$

and Eq. (24) with the assumption $D/F = 0$ in the SU(3) vector meson octet. Using the known values for $g^2_{\rho NN}/4\pi = 0.7 - 1.3$ [18] and $g^2_{\omega NN}/4\pi = 22 - 24$ [18], one may obtain $-g_{\phi NN} = 0.57 - 0.65$ and $-g_{\phi NN} = 1.07 - 1.09$ for the expressions (25) and (24), respectively. On the other hand, the theoretical estimates of Ref. [24] give $g_{\phi NN} = -0.24$. Thus, we can conclude that even using the standard OZI rule violation (thought non-ideal $\omega - \phi$ mixing) one is left with estimated values of $g_{\phi NN}$ within a quite large interval. The possible hidden strangeness in a nucleon may even increase this interval. In this paper we restrict ourselves to the standard OZI rule violation mechanisms and analyze consequences of varying $-g_{\phi NN}$ in the region $0.0 - 1.0$.

The negative coupling constant $g_{\phi\rho\pi}$ results in a destructive interference between meson exchange amplitudes (a) and direct emission (b) in Figs. 1 and 2. Analyzing the unpolarized

$\pi^- p \to n\phi$ reaction, based on the data of Ref. [14], we find that the yet unconstrained three parameters $g_{\phi NN}$, $\Lambda^\rho_{\phi\rho}$, $\Lambda_N$ become related to each other as $\Lambda^\rho_{\phi\rho}=\Lambda^\rho_{\phi\rho}(g_{\phi NN}, \Lambda^\rho_{\phi\rho})$ by the constrains given by the data, and two solutions emerge for this dependence: (i) $\sigma_{(a)} > \sigma_{(b)}$ and (ii) $\sigma_{(a)} < \sigma_{(b)}$, where $\sigma_{(a,b)}$ are the total cross section for the meson exchange process (a) and the direct $\phi$ emission (b) calculated separately. These solutions are displayed in Fig. 3 for several values of $g_{\phi NN}$ as discussed above.

In order to constrain one more free parameter we analyze also the cross section $d\sigma/d\Omega$ for the $pp \to pp\phi$ reaction, using simultaneously the DISTO data [10,11], i.e. the angular distribution [10] (we remind that in our notation $\Omega$ is the $\phi$ meson solid angle) and the total cross section [11], respectively. For this aim we fix the absolute normalization of the angular distribution $d\sigma/d\Omega$ given in Ref. [10] by making use of the recently published the total cross section [11]. As a result we get the fat dots in Fig. 3. The minimum values for $-g_{\phi NN}$ are 0.07 (for $\sigma_{(a)} > \sigma_{(b)}$) and 0.60 (for $\sigma_{(a)} < \sigma_{(b)}$), respectively at $\Lambda_N \to \infty$. For both solutions we find that increasing values of $|g_{\phi NN}|$ results in decreasing values of $\Lambda_N$ leaving the total cross section or "integrated" strength of the $\phi NN$ interaction on the same level.

To explore in more detail the relative importance of the direct $\phi NN$ interaction we now employ three parameter sets; two of them correspond to the $\sigma_{(a)} > \sigma_{(b)}$ solution and the third one to $\sigma_{(a)} < \sigma_{(b)}$:

set A: $g_{\phi NN} = -0.24$ [24], $\Lambda^\rho_{\phi\rho} = 1.34$ GeV, $\Lambda_N = 1.065$ GeV $(\sigma_{(a)} > \sigma_{(b)})$,

set B: $g_{\phi NN} = -0.8$, $\Lambda^\rho_{\phi\rho} = 1.34$ GeV, $\Lambda_N = 0.715$ GeV $(\sigma_{(a)} > \sigma_{(b)})$,

set C: $g_{\phi NN} = -0.8$, $\Lambda^\rho_{\phi\rho} = 1.60$ GeV, $\Lambda_N = 1.99$ GeV $(\sigma_{(a)} < \sigma_{(b)})$.

In the sets B and C we choose $-g_{\phi NN}$ close to its upper limit as predicted by SU(3) symmetry.

Results of our calculation of the total cross section for the $\pi^- p \to n\phi$ reaction for these parameter sets are shown in Fig. 4 as a function of the energy excess $\Delta s^{\frac{1}{2}} \equiv s^{\frac{1}{2}} - s_{0\pi N}^{\frac{1}{2}}$ with $s_{0\pi N} = (M_N + m_\phi)^2$. The contribution of the meson exchange channel (a) is displayed separately by the dot-dashed line, and the direct emission by the nucleon line (b) is depicted by the dashed line. Clearly seen is the strong destructive interference of the channels (a) and (b), in particular for the set C.

In Figs. 5 and 6 we display results of our calculations for $d\sigma/d\Omega$ for the $pp \to pp\phi$ reaction together with the available data [10,11] for the parameter sets B and C, respectively, at $\Delta s^{\frac{1}{2}} = s^{\frac{1}{2}} - s_{0\,NN}^{\frac{1}{2}} = 82$ MeV with $s_{0\,NN} = (2M_N + m_\phi)^2$. The results for the set A are very similar to that of the set B and we do not separately display them here. Interestingly, in all parameter sets considered the channel (a) dominates in the $NN \to NN\phi$ reaction, but the interferences are different for different parameter sets.

One can see a qualitative difference in $\pi N$ and $NN$ reactions for the set C. In the $\pi N$ reaction the direct radiation channel (b) is dominant, i.e. $\sigma_{(b)} > \sigma_{(a)}$. In contrast, in the $NN$ reaction the relative contribution of the direct emission channel (b) increases considerably as compared with sets A and B, but it is still smaller that the meson exchange channel (a). The reason for this difference is the following one. The direct emission (b) in the reaction $\pi N$ consists of the two competing u-channel and s-channel diagrams shown in Fig. 1b. which add destructively, while the contribution of the of the u-channel amplitude is greater. However, the corresponding contributions of the two competing diagrams in Fig. 2b are numerically nearly the same resulting in a stronger suppression of the direct channel (b).

As we have adjusted our parameters by the data, it is clear that they describe the data with approximately equal quality, and at the present level of the data accuracy it is difficult to give a preference to one of them. Therefore, we now investigate whether other observables can be used to constrain the parameters further and whether the difference between $pp$ and $pn$ reactions is a sensible measure.

## B. $\pi^- p \to n\phi$ reaction

The calculated angular differential cross sections of the $\pi^- p \to n\phi$ reaction at $\Delta s^{\frac{1}{2}} = 50$ MeV and for the parameter sets A, B, C are shown in Fig. 7. One can see that the shapes of the distributions for the sets A and B are very similar to each other. They are quite smooth and close to the distribution of the meson exchange channel (a). Only in the backward direction the total cross section slightly decreases due to the destructive interference with

the direct channel (b), leading to some enhancement of the cross section in forward direction. (We would like to mention here, that the extrapolated value of the $\phi$ production cross section in $NN$ reactions [16] from the data [10] would require somewhat different parameter sets, which in turn cause also more pronounced differences between the sets A and B.) Contrary to that, for the model C the largest destructive interference appears at forward direction, where the contributions of the two competing channels (a) and (b) are close to each other. As a result, the cross section is enhanced in the backward direction. So we can conclude that the differential cross section is sensitive to the dynamics of the $\phi$ production and the direct $\phi NN$ coupling (a similar conclusion for $\omega$ production has arrived at in Ref. [26]).

The prediction for spin density matrix elements $\rho_{00}$ and $\rho_{11}$ for the different models is shown in Fig. 8 as a function of the $\phi$ production angle in c.m.s. at $\Delta s^{\frac{1}{2}} = 50$ MeV. The sets A and B deliver standard values, typical for the spin-flip processes, i.e. $\rho_{00} \simeq 0$, $\rho_{11} \simeq 0.5$. But the parameter set C predicts a strong deviation from these values, especially at forward direction. The reason of this effect is the following. In the meson exchange channel (a) the nucleon spin-flip amplitudes result in transitions $m_i \rightarrow m_\phi, m_f$, where $m_f = m_i - m_\phi$ with $m_\phi = \pm 1$. For instance, the transitions like $-\frac{1}{2} \rightarrow -1, \frac{1}{2}$ are dominant. In the direct radiation channel (b) together with this strong amplitudes we have finite amplitudes for the transition $m_i \rightarrow 0, m_f$, where $m_f = m_i$. In the set C the strongly competing nucleon spin flip amplitudes cancel each other and only the nucleon spin conserving direct emission amplitude (b) survives. This is illustrated in Fig. 9, where we show the nucleon spin flip (left panel) and the nucleon spin conserving (right panel) amplitudes for the set C. Here $F_z = \mathrm{Im} T^{\pi p \rightarrow n\phi}$ with the quantization axis along the $\mathbf{z}$ direction ($T^{\pi p \rightarrow n\phi}$ is purely imaginary).

The anisotropies of the decay channels $\phi \rightarrow e^+ e^-$ and $\phi \rightarrow K^+ K^-$ (cf. Eqs. (5, 6) for the different parameter sets are shown in Fig. 10. Again, one can see a strong deviation of our prediction for the set C from the naive expectation $B^{e^+ e^-} \simeq 1$, $B^{K^+ K^-} \simeq -1$ based on a purely mesonic exchange channel or on the sets A and B. Fig. 11 illustrates the the manifestation of this deviation in the real $e^+ e^-$ and $K^+ K^-$ angular distributions. The distributions $W_L$ and $W_T$ are the longitudinal (along the quantization axis) and transversal

15

fluxes for the outgoing electrons or kaons. The functions $W_L$ and $W_T$ are normalized as $\int \sqrt{W_L^2(\Theta) + W_T^2(\Theta)} d\cos\Theta = 1$, where $\Theta$ is defined by Eq. (5). Thus, one can see that the sets A and B predict a practically vanishing kaon flux in the longitudinal direction for all $\phi$ production angles. The set C predicts a finite amount of the longitudinal flux which increases with decreasing $\phi$ production angle in c.m.s. A corresponding modification is predicted for the electron flux too.

## C. $pp \to pp\phi$ and $pn \to pn\phi$ reactions

As shown in Figs. 5 and 6 the meson exchange contribution (a) is the dominating contribution to the $NN \to NN\phi$ reaction, therefore, it is useful to recall the threshold prediction for this channel in the absence of the final state interaction, which serves as a starting point for further calculations at finite energy. Adopting the notation of Ref. [17] we can express the invariant amplitudes of the reaction $ab \to ab\phi$ with $a = p$, $b = p$ or $n$ as following

$$T_{pp} = F_1, \qquad T_{pn} = \frac{1}{2}(F_0 + F_1), \qquad (27)$$

where $F_0$ $(F_1)$ is the initial singlet (triplet) amplitude with

$$F_0 = f_0(-1)^{\frac{1}{2}+m_a} \delta_{-m_a m_b}(\delta_{\frac{1}{2}m_c} \delta_{\frac{1}{2}m_d} - \delta_{-\frac{1}{2}m_c} \delta_{-\frac{1}{2}m_d}),$$
$$F_1 = f_1(-1)^{\frac{1}{2}+m_a} \delta_{m_a m_b}(\delta_{\frac{1}{2}m_c} \delta_{-\frac{1}{2}m_d} - \delta_{-\frac{1}{2}m_c} \delta_{\frac{1}{2}m_d}), \qquad (28)$$

where $m_{a,b}$ and $m_{c,d}$ are again the nucleon spin projections in the initial and final states, respectively, $f_0 = 6\sqrt{2}T_0$, $f_1 = 2\sqrt{2}T_0$, where the threshold amplitude $T_0$ is defined by Eq. (25) in Ref. [9]. The above equations lead to the ratio $f_0/f_1 = 3$ and to the ratio of singlet to triplet cross sections

$$\frac{|F_0|^2}{|F_1|^2} = 9. \qquad (29)$$

The beam target asymmetries (8) read $C_{BT\,pp} = 1$, and $C_{BT\,pn} = -0.8$. The ratio of the total cross sections in $pn$ and $pp$ reactions is 5. Accordingly, the prediction for the spin density [17] reads $\rho_{00} = 0$, $\rho_{11} = 0.5$.

Let us now turn back to the Figs. 5 and 6. These figures show (i) a relatively small contribution of the direct radiation channel (b), which is in agreement with previous works [9,15], (ii) the cross sections for the $pn$ interaction are qualitatively very similar in shape to these of the $pp$ interaction but they are larger, and (iii) the ratio of the corresponding cross sections in $pn$ and $pp$ reactions is different for the sets A (or B) and C. Later we will discuss this aspect in detail.

The energy dependence of the total cross sections of $pp \to pp\phi$ and $pn \to pn\phi$ reactions for the sets B and C is shown in Figs. 12 and 13. We do not display the result for the set A because it is practically the same as for the set B. The experimental data is taken from Ref. [11]. One can see that the direct radiation channel (b) is much indeed smaller than the meson exchange contribution (a) in the near-threshold region where our consideration is valid.

Fig. 14 shows the energy dependence of the ratio of the total cross sections of $pp \to pp\phi$ and $pn \to pn\phi$ reactions for the different parameter sets. One can see that this ratio increases with the energy excess and differs from the threshold value 5 in case of absence of FSI. The FSI is greater in the triplet initial (or singlet final) states and reduces the contribution of the initial singlet state in the $pn$ interaction. For the set C the ratio $\sigma_{pn}/\sigma_{pp}$ is greater because of the relatively greater contribution of the initial triplet state in the meson exchange channel (a). Fig. 15 shows the energy dependence of the ratio of the singlet to triplet cross sections in $pn$ interactions (cf. Eq. (29)). The left panel shows this ratio for the separate channels, while on the right panel one can see our prediction for this ratio for the different parameters sets. One can again see a strong deviation from the threshold prediction (29) without FSI and non-trivial non-monotonic dependence of these ratios with some maximum values around $\Delta s^{\frac{1}{2}} \sim 20$ MeV.

Fig. 16 shows beam target asymmetry (8) for the separate channels for $pp$ and $pn$ interactions. For the $pp$ interaction it coincides with its threshold value $C_{BT} = 1$ up to a relatively large energy excess. For the $pn$ interaction the asymmetry is different for the different channels which reflects the different role of the singlet and triplet states in the

different amplitudes which are additionally modified by the FSI.

The total asymmetry for the different parameter sets is shown in Fig. 17. It is interesting that even for the sets A and B with small contribution of the direct radiation amplitude (b) the asymmetry for $pn$ interaction strongly deviates from the threshold prediction (without FSI: $C_{BT}^{pn} = -0.8$), displaying a minimum around $\Delta s^{\frac{1}{2}} \sim 20$ MeV.

We do not display here our results for the spin density matrix elements because for the sets A, B and C we get almost the threshold values, i.e. $\rho_{00} = 0$, $\rho_{11} = 0.5$, which reflects the dominance of the meson exchange channel (a).

## V. SUMMARY

We have analyzed the $\phi$ production in $\pi N$ and $NN$ interactions in the near-threshold region using the conventional "non-strange" hadron dynamics, based on the amplitudes allowed by non-ideal $\omega - \phi$ mixing, that is meson conversion in a $\phi\pi\rho$ vertex and direct $\phi$ emission from the nucleon legs by a direct $\phi NN$ coupling. Using the limited body of available experimental data of the total unpolarized reactions we have tried to reduce as much as possible the uncertainty of the model parameters. As a result we get two branches of solutions with either a relatively small or a relatively large contribution of the direct emission channel which is determined by the strength of the $\phi NN$ interaction. By making use of these solutions we have compared various parameter sets with different strengths of the direct $\phi NN$ interaction.

Analyzing the $\pi p \to n\phi$ reaction we find a strong dependence of the various observables on the strength of the $\phi NN$ interaction. The study of the differential cross section and angular distributions of electrons and kaons in the $\phi \to e^+e^-$ and $\phi \to K^+K^-$ decays seems to be most promising in investigating the $\phi NN$ dynamics. Experimentally, this study might be performed with the pion beam at the HADES spectrometer in GSI/Darmstadt.

Analyzing the $NN \to NN\phi$ reaction we find a large difference in $pp$ and $pn$ reactions due to the different role of the singlet and triplet nucleon spin states in the entrance channel and

18

strong final state interaction. We predict a non-monotonic energy dependence of the ratio $\sigma_{pn}/\sigma_{pp}$ and of the beam target asymmetry for the $pn$ interaction which deviates strongly from the pure threshold prediction.

Finally, we emphasize once more that the present investigation is completely based on the conventional meson-nucleon dynamics and, therefore, our predictions may be considered as a necessary background for forthcoming studies of the strangeness degrees of freedom in non-strange hadrons. Additionally we would like to mention that fixing the $\phi NN$ coupling is important for an access to the elastic $\phi N$ scattering cross section which determines the degree of thermalization and collective flow properties of the $\phi$ mesons in heavy-ion collisions at SIS energies.

## APPENDIX A: FINAL STATE INTERACTION

In this appendix we present the formulae for the FSI and corresponding correction factors. We use the general framework for the FSI enhancement factor based on the Jost function formalism. Important aspects of this framework are described in the monograph by Gillespie [27] and some early original papers [28]. With respect to the significance of this problem in studying various near-threshold particle production reactions in the present time with cooled beams, we accumulate here the relevant expressions of this method and give the final result in a form convenient for specific calculations. For the Jost function formalism we use the notation of the textbook by Newton [29]. For simplicity, we limit our consideration to

the s-wave interaction which is dominant in the near-threshold region. A generalization for higher angular momenta may be done straightforwardly.

The FSI enhancement factor for two identical particles with momentum $k$ in their c.m.s. reads

$$\mathcal{I} = \frac{1}{\mathcal{J}_+(k)}, \tag{A1}$$

where $\mathcal{J}_+$ belongs to a set of functions $\mathcal{J}_\pm(k)$ which are defined through the Wronskian of two linearly independent solutions of the Schrödinger equation,

$$\mathcal{J}_\pm(k) = f_\pm(k,r)\,\varphi'(k,r) - f'_\pm(k,r)\,\varphi(k,r), \tag{A2}$$

where the prime means here the derivative with respect to $r$. The function $\mathcal{J} = \mathcal{J}_+$ is called the Jost function. The integral equations for the regular and irregular functions $\varphi(k,r)$ and $f_\pm(k,r)$ have the standard form

$$\varphi(k,r) = \frac{\sin kr}{k} + \frac{1}{k}\int_0^\infty dr'\,\sin k(r-r')V(r')f_\pm(k,r'),$$
$$f_\pm(k,r) = e^{\pm kr} - \frac{1}{k}\int_0^\infty dr'\,\sin k(r-r')V(r')f_\pm(k,r'). \tag{A3}$$

Eq. (A2) and the boundary conditions $\varphi(0) = 0$, $\varphi'(0) = 1$ show that $\mathcal{J}_\pm(k) = f_+(k,0)$, thus allowing the integral representation

$$\mathcal{J}(k) = 1 + \frac{1}{k}\int_0^\infty dr\,\sin kr V(r)f_+(k,r). \tag{A4}$$

The physical wave function $\psi^+(k,r)$ is related to the regular function $\varphi(k,r)$ as

$$\psi^+(k,r) = \frac{k\varphi(k,r)}{\mathcal{J}(k)}, \tag{A5}$$

which means that the inverse of the square of the modulus of $\mathcal{J}(k)$ measures the probability of finding the particles near $r = 0$, relative to a situation without interaction. From Eq. (A4) one can find the important asymptotic condition

$$\lim_{|k|\to\infty} \mathcal{J} = 1, \tag{A6}$$

20

which shows that at high energies the enhancement tends to unity, thus leaving the total amplitude unchanged.

The analyticity of $\mathcal{J}$ together with the asymptotic condition Eq. (A6) leads to the integral representation of the Jost function in terms of the phase shift $\delta(k)$

$$\mathcal{J}(k) = \prod_n \left(1 + \frac{\kappa_n^2}{k^2}\right) \exp\left[\frac{1}{\pi} \int_{-\infty}^{\infty} dk' \frac{\delta(k')}{k - k' + i\epsilon}\right], \tag{A7}$$

where $\kappa_n$ is related to the corresponding binding energy $\kappa_n^2 = -2\mu\epsilon_n > 0$ if bound states appear; $\mu$ is the corresponding reduced mass.

For the practical usage of the above formalism it is convenient to work with the effective potentials which give an exact analytical expression for the phase shift. Let us first consider the singlet $NN$ scattering (without bound state). The Eckart potential

$$V(r) = -\frac{8\alpha^2}{\alpha^2 - \beta^2} \left(\frac{e^{-\alpha r}}{\alpha - \beta} + \frac{e^{\alpha r}}{\alpha + \beta}\right)^{-2}, \quad \alpha > 0, \beta > 0, \tag{A8}$$

gives the $s$-wave phase shift

$$k \cot \delta_0 = \frac{\alpha\beta}{\alpha - \beta} + \frac{k^2}{\alpha - \beta} \tag{A9}$$

reproducing the effective-range phase shift exactly,

$$k \cot \delta_0 = -\frac{1}{a_0} + \frac{1}{2} r_0 k^2, \tag{A10}$$

with

$$\alpha = \frac{1}{r_0}\left(\sqrt{1 - 2r_0 a_0^{-1}} + 1\right), \quad \beta = \frac{1}{r_0}\left(\sqrt{1 - 2r_0 a_0^{-1}} - 1\right). \tag{A11}$$

The insertion of $\delta_0$ from (A9),

$$\delta_0 = \frac{i}{2} \ln\left[\frac{(k - i\alpha)(k + i\beta)}{(k + i\alpha)(k - i\beta)}\right], \tag{A12}$$

in Eq. (A7) gives the analytical expression for the Jost function

$$\mathcal{J}(k) = \frac{k + i\beta}{k + i\alpha}, \tag{A13}$$

21

and the resulting enhancement factor for singlet interaction reads therefore as

$$\mathcal{I}_0(k) = C_0(k^2) \, \frac{\sin \delta_0 \, e^{i\delta_0}}{k},$$

$$C_0(k^2) = \frac{k^2 + \alpha^2}{\alpha - \beta} = \frac{(kr_0)^2 + 2\left(1 - r_0 a_0^{-1} + \sqrt{1 - 2r_0 a_0^{-1}}\right)}{2r_0}, \tag{A14}$$

which coincides with the classical Watson enhancement factor [30]

$$\mathcal{I}_W(k) = C_W \, \frac{\sin \delta_0 \, e^{i\delta_0}}{k} \tag{A15}$$

in the limit of $kr_0 \to 0$. Note that expression (A15) is commonly used in calculations of the FSI in the near-threshold region (cf. [31]), where the constant $C_W$ is fixed by a comparison of calculation and experimental data. Eq. (A14) is superior to Eq. (A15) because it yields a definite value of $C_W = C_0(k^2 = 0)$ by making use of the independent phase shift data and satisfies at the same time the required asymptotic behavior according to Eq. (A6),

$$\lim_{|k|\to\infty} \mathcal{I}_0(k) = 1, \tag{A16}$$

contrary to Eq. (A15), where $\mathcal{I}_W(k) \to 0$ at $|k| \to \infty$.

Fig. 18 illustrates the effect of FSI when using different enhancement factors for our parameter set B for the reaction $pp \to pp\phi$, where we keep here only the dominant mesonic exchange diagram in Fig. 2a and use the threshold value. In this case the energy dependence comes only from the enhancement factor and the phase space volume. The cross section calculated with enhancement factors from Eqs. (A14) and (A15) with $C_W = C_0(0)$ are shown by the dashed and the solid lines, respectively. For comparison we show also the cross section calculated without FSI (dot-dashed line). One can see, that the difference between the two factors (A14) and (A15) is indeed negligible at sufficiently small energy excess, say at $\Delta s^{\frac{1}{2}} < 10$ MeV with $kr_0 \ll 1$, where the Watson theory [30] is valid, thus supporting the approach of [31]. At $\Delta s^{\frac{1}{2}} > 50$ MeV the difference between the two variants results in a factor 2 and greater.

Following Ref. [29], for the triplet $pn$ interaction one can use the effective potential of the Bargmann type

$$V(r) = -4\kappa \frac{d}{dr} \left[ \text{sh}\, \alpha_1 r \frac{g(\kappa, r)}{g(\kappa + \alpha_1, r) - g(\kappa - \alpha_1, r)} \right],$$
$$g(q, r) = \left( e^{-qr} + 2\text{sh}\, qr \right) k^{-1} \tag{A17}$$

which reproduces the known phase shift and the deuteron binding energy. The Jost function in this case reads

$$\mathcal{J}(k) = \frac{k - i\kappa}{k + i\alpha_1}, \tag{A18}$$

with

$$\alpha_1 = (2 - \kappa r_1) r_1^{-1}, \tag{A19}$$

where $\kappa^2 = 2\mu\epsilon_d$, $\epsilon_d$ is the deuteron binding energy, and $r_1$ and $a_1 = (\kappa(1 - \kappa r/2))^{-1}$ are the triplet effective radius and scattering length, respectively. The triplet enhancement factor reads explicitly

$$\mathcal{I}_1(k) = C_1(k^2) \frac{\sin \delta_1\, e^{i\delta_1}}{k},$$
$$C_1(k^2) = \frac{k^2 + \alpha_1^2}{\alpha_1 + \kappa} = \frac{(kr_1)^2 + 2\left(1 - r_1 a_1^{-1} + \sqrt{1 - 2r_1 a_1^{-1}}\right)}{2r_1}, \tag{A20}$$

In our calculation we use $a_{0,1}$ and $r_{0,1}$ from Ref. [33]

$$pn \ \text{singlet}: \quad a_{0pn} = -23.768\,\text{fm}, \quad r_{0pn} = 2.75\,\text{fm},$$

$$pp \ \text{singlet}: \quad a_{0pp} = -7.8098\,\text{fm}, \quad r_{0pp} = 2.767\,\text{fm},$$

$$pn \ \text{triplet}: \quad a_{1pn} = \phantom{-}5.424\,\text{fm}, \quad r_{1pn} = 1.759\,\text{fm}, \quad \kappa^{-1} = 4.318\,\text{fm}. \tag{A21}$$

Finally, we would like to mention that the approach presented here is equivalent to the approach in Ref. [32] if the off-shell correction factor $\mathcal{P}$ (cf. Eq. (9) in [32]) takes the form $\mathcal{P}(E, k) = -a_x r_x^{-1} \left( 1 + \sqrt{1 - 2r_x a_x^{-1}} \right)$ with $x = 0, 1$.

# REFERENCES

[1] J. Ellis, M. Karliner, D.E. Kharzeev and M.G. Sapozhnikov, Phys. Lett. B **353**, 319 (1995).

[2] S. Okubo, Phys. Lett. B **5** (1963) 165;
G. Zweig, CERN report No. 8419/TH 412 (1964);
I. Iizuka, Prog. Theor. Phys. Suppl. **37/38** (1966) 21.

[3] M.P. Locher and Y. Lu, Z. Phys. A **351**, 83 (1995);
D. Buzatu and F.M. Lev, Phys. Lett. B **329**, 143 (1994).

[4] J. Gasser, H. Leutwyler and M.E. Sainio, Phys. Lett. B **253**, 252 (1991).

[5] D.B. Kaplan and A.V. Manohar, Nucl. Phys. B **310** 527 (1988);
R.D. McKeown, Phys. Lett. B **219**, 140 (1989);
E.M. Henley, G. Krein, S.J. Pollock and A.G. Williams, Phys. Lett. B **269**, 31 (1991).

[6] A.I. Titov, Y. Oh and S.N. Yang, Phys. Rev. Lett. **79**, 1634 (1997);
A.I. Titov, Y. Oh, S.N. Yang and T. Morii, Phys. Rev. C **58**, 2429 (1998).

[7] J. Ellis, M. Karliner, D.E. Kharzeev and M.G. Sapozhnikov, hep-ph/9909235.

[8] W.S. Chung, G.Q. Li and C.M. Ko, Phys. Lett. B **401**, 1 (1997).

[9] A.I. Titov, B. Kämpfer, V.V. Shkyar, Phys. Rev. C **59**, 999 (1999).

[10] F. Balestra et al. (DISTO Collaboration), Phys. Rev. Lett. **81**, 4572 (1998).

[11] F. Balestra et al. (DISTO Collaboration), Phys. Lett. B **468**, 7 (1999).

[12] N. Herrmann (FOPI collaboration), Nucl. Phys. A 610 (1996) 49c,
A. Mangiarotti, invited talk at the FOPI collaboration meeting, Obernai, France, Sep. 29 - 30, 1999,
R. Kotte, private communication

[13] J. Friese et al. (HADES collaboration), GSI report 97-1, p. 193 (1997).

[14] A. Baldini et al., *Total cross sections of high energy particles*, Springer-Verlag, Heidelberg, 1988.

[15] K. Nakayama, J.W. Durso, J. Haidenbauer, C.Hanhart and J. Speth, Phys. Rev. C **60**, 055209 (1999).

[16] F. Hibou et al., Phys. Rev. Lett. **83**, 492 (1999).

[17] M.P. Rekalo, J. Arvieux and E. Tomasi-Gustafsson, Z. Phys. A **357**, 133 (1997).

[18] R. Machleidt, Adv. Nucl. Phys. **19**, 189 (1989).

[19] H. Haberzettl, Phys. Rev. C **56**, 2041 (1997);
H. Haberzettl, C. Bennhold, T. Mart and T. Feuster, Phys. Rev. C **58**, 40 (1998).

[20] M. Schäfer, H.C. Dönges, A. Engel and U. Mosel, Nucl. Phys. A **575**, 429 (1994).

[21] A.I. Titov, B. Kämpfer and E. Bratkovskaya, Phys. Rev. C **51**, 227 (1995).

[22] A. Engel, R. Shyam, U. Mosel and A.K. Dutt-Mazumder, Nucl. Phys. A **603**, 387 (1996);
V.V. Shklyar, B. Kämpfer, B.L. Reznik and A.I. Titov, Nucl. Phys. A **628**, 255 (1998).

[23] A.I. Titov, T.-S.H. Lee, H. Toki and O. Streltsova, Phys. Rev. C **60**, 035205 (1999).

[24] U.-G. Meissner, V. Mull, J. Speth and J.W. Van Orden, Phys. Lett. B **408**, 381 (1997).

[25] J.J. De Swart, Rev. Mod. Phys. **35**, 916 (1963).

[26] K. Nakayama, A. Szczurec, C. Hanhart, J. Haidenbauer and J. Speth, Phys. Rev. C **57** 1580 (1998).

[27] J. Gillespie, *Final-State Interactions*, Holden-Day Advanced Physics Monographs, 1964.

[28] R. Jost and W Kohn, Phys. Rev. **87**, 977 (1952);

V. Bargmann, Rev. Mod. Phys. **21**, 488 (1949);

E. Fermi, Suppl. Nuovo Cimento, **2**, 17 (1955);

R.G. Newton, Phys. Rev. **105**, 763 (1957); **107**, 1025 (1957).

[29] R.G. Newton, *Scattering Theory of Particles and Waves*, McGrow-Hill Inc., 1966.

[30] K.M. Watson, Phys. Rev. **88**, 1163 (1952); *Scattering Theory of Particles and Waves*, McGrow-Hill Inc., 1966.

[31] N. Kaiser, Phys. Rev. C **60**, 057001 (1999);

V. Bernard, N. Kaiser and Ulf-G. Meissner, Eur. Phys. J. A **4**, 259 (1999).

[32] C. Hanhart and K. Nakayama, Phys. Lett. B **454**, 176 (1999).

[33] O. Dumbrajs, R. Koch, H. Pilkuhn, G.C. Oades, H. Behrens, J.J. De Swart and P. Kroll, Nucl. Phys. B **216**, 277 (1983).

FIGURES
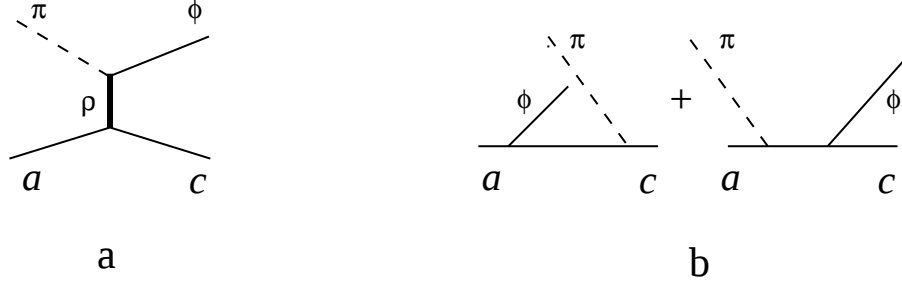


FIG. 1.    Diagrammatic representation of the $\pi N \to N\phi$ reaction mechanisms: (a) meson exchange diagram with $\phi$ emission from the $\phi\rho\pi$ vertex, (b) direct $\phi$ emission from the $\phi NN$ vertex in Compton like diagrams.
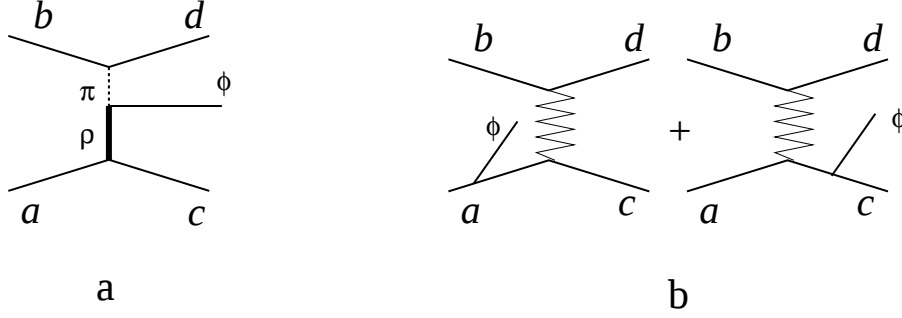


FIG. 2.    Diagrammatic representation of the $NN \to NN\phi$ reaction mechanisms: (a) meson exchange diagram with $\phi$ emission from the internal meson conversion in the $\phi\rho\pi$ vertex, (b) direct $\phi$ emission from nucleon legs.  The zig-zag lines depict effective boson exchange.  Exchange diagrams are not displayed.
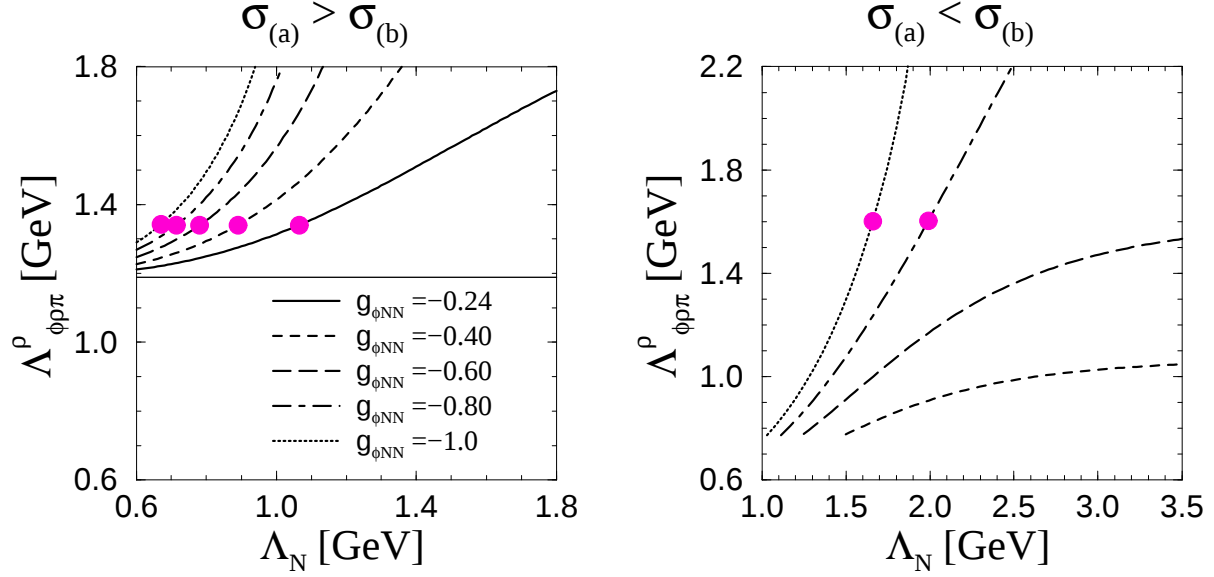
FIG. 3. Solutions for the function $\Lambda^{\rho}_{\phi\rho}=\Lambda^{\rho}_{\phi\rho}(g_{\phi NN}, \Lambda^{\rho}_{\phi\rho})$; left panel: $\sigma_{(a)} > \sigma_{(b)}$, right panel: $\sigma_{(a)} < \sigma_{(b)}$. The thin straight solid line in the left panel corresponds to $g_{\phi NN} = 0$. Further explanations are given in the text.
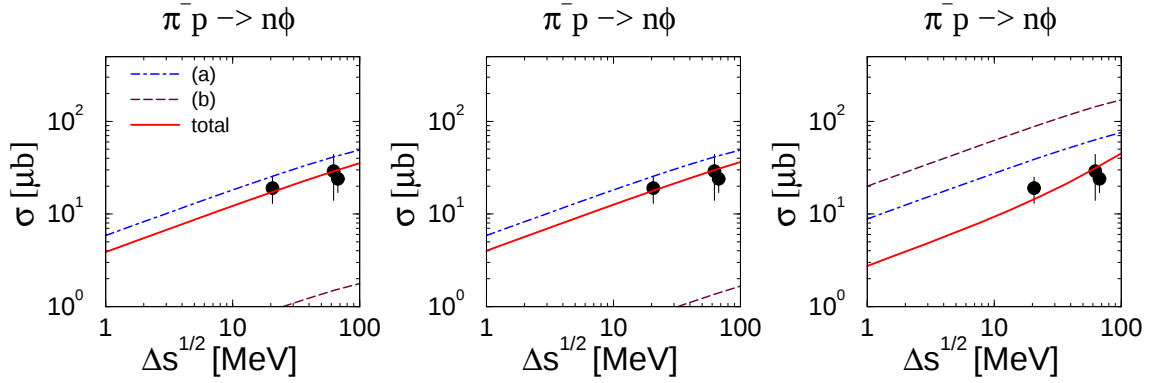


FIG. 4. The total cross section for the $\pi^- p \to n\phi$ reaction for the parameters sets A, B, C (left, middle, right panels) as a function of the energy excess $\Delta s^{\frac{1}{2}}$. Data from [14].

28
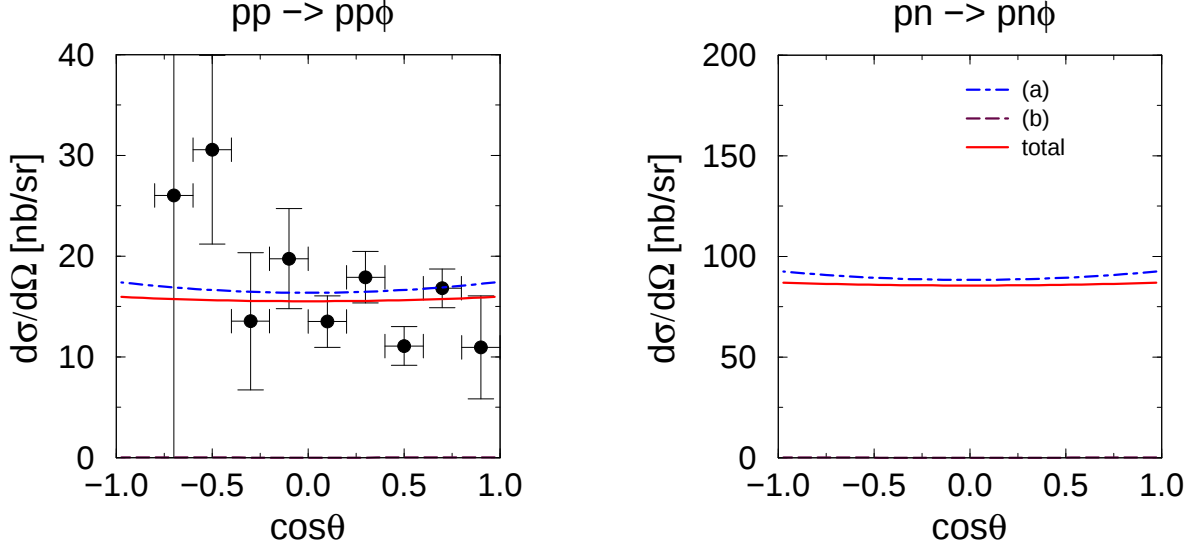
FIG. 5. The angular distribution $d\sigma/d\Omega$ for $NN \to NN\phi$ reactions for parameter set B for $pp$ (left panel; data from [10] with normalization according to [11]) and $pn$ (right panel) interactions.
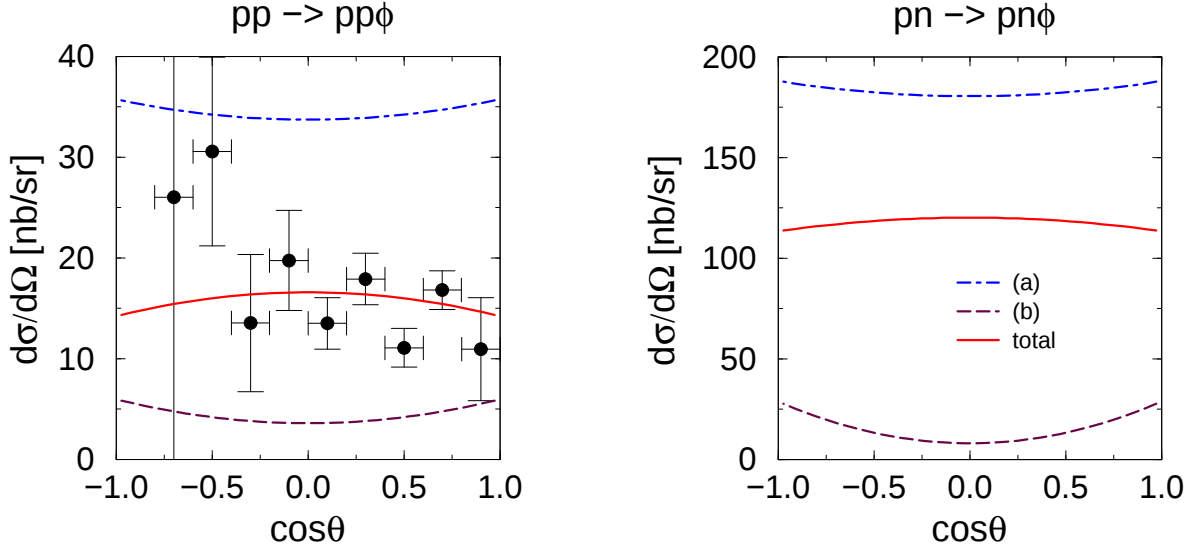


FIG. 6. The same as in Fig. 5, but for parameter set C.
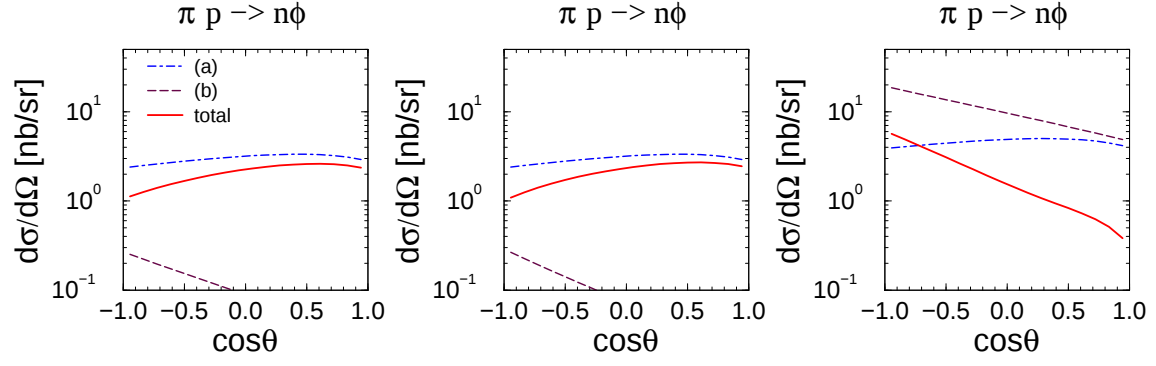
FIG. 7. The differential cross sections for the $\pi^- p \to n\phi$ reaction at $\Delta s^{\frac{1}{2}} = 50$ MeV for the same parameter sets as in Fig. 4.
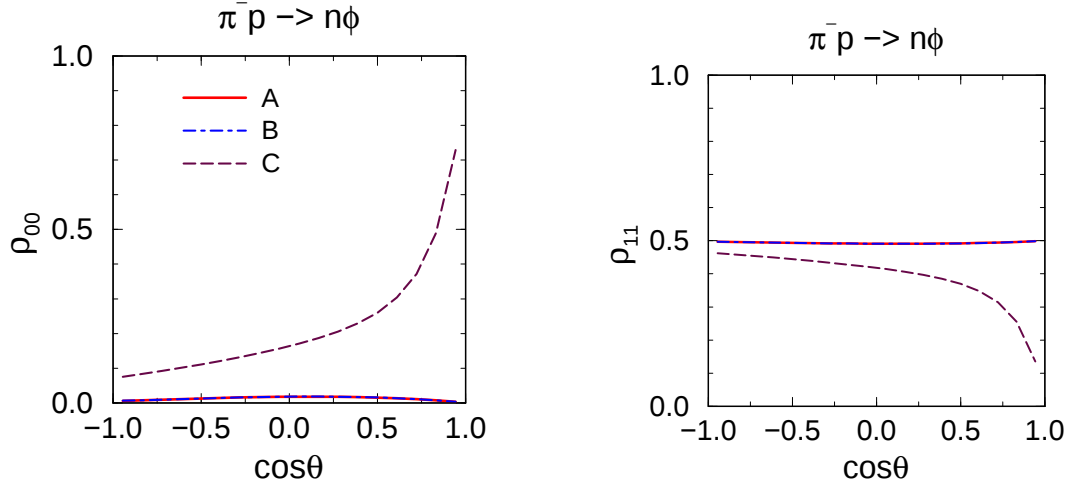


FIG. 8. The spin density matrix elements $\rho_{00}$ (left panel) and $\rho_{11}$ (right panel) for the different parameter sets at $\Delta s^{\frac{1}{2}} = 50$ MeV.
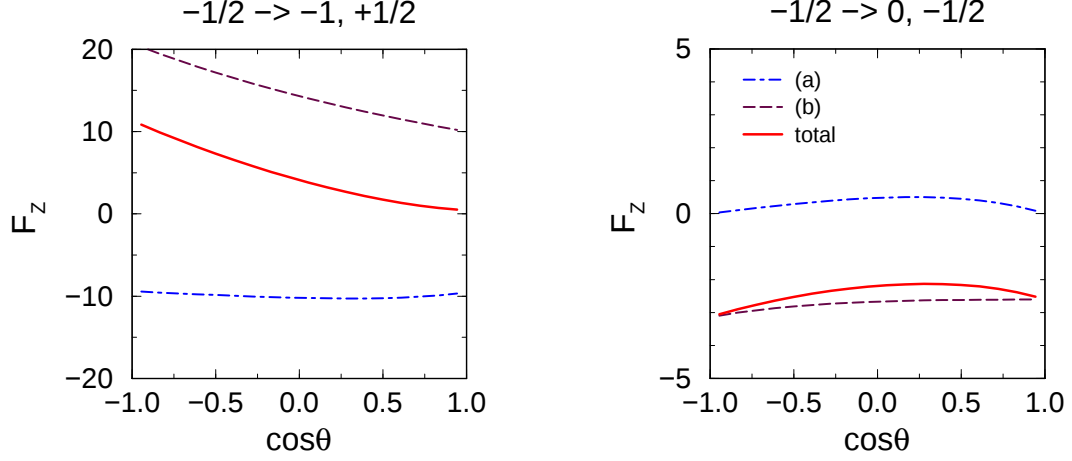
FIG. 9. The nucleon spin flip (left panel) and spin conserving (right panel) amplitudes $F_z$ for the parameter set C.
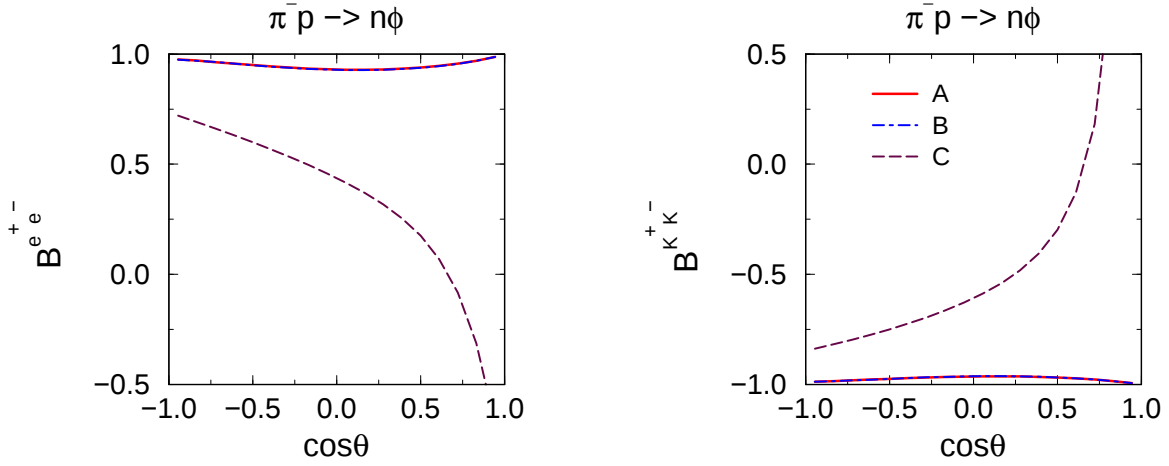


FIG. 10. The anisotropies in the reactions $\phi \to e^+ e^-$ (left panel) and $\phi \to K^+ K^-$ (right panel) for different parameter sets.
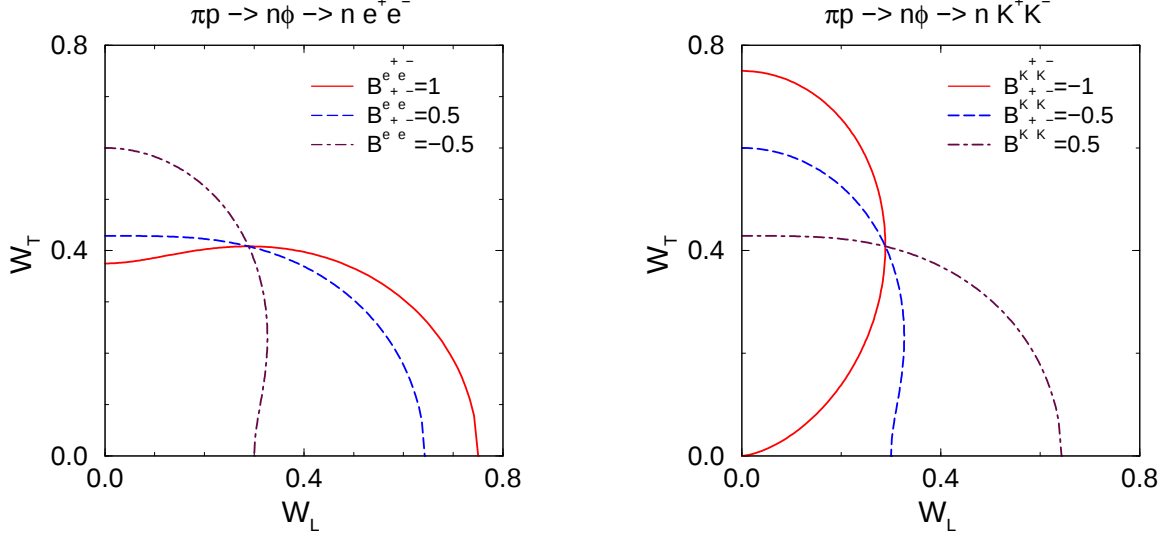
FIG. 11.    The longitudinal ($W_L$) and transversal ($W_T$) fluxes of the outgoing electrons (left panel) or kaons (right panel) for various values of the anisotropies.
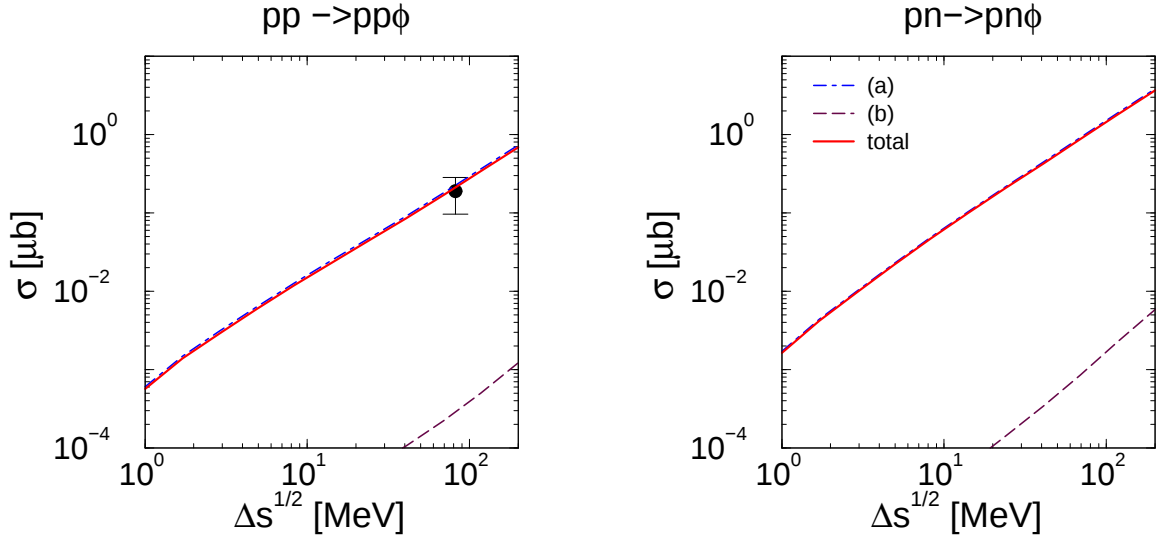


FIG. 12.    The energy dependence of the total cross sections of $pp \rightarrow pp\phi$ (left panel) and $pn \rightarrow pn\phi$ (right panel) reactions for the parameter set B. Data from [11].
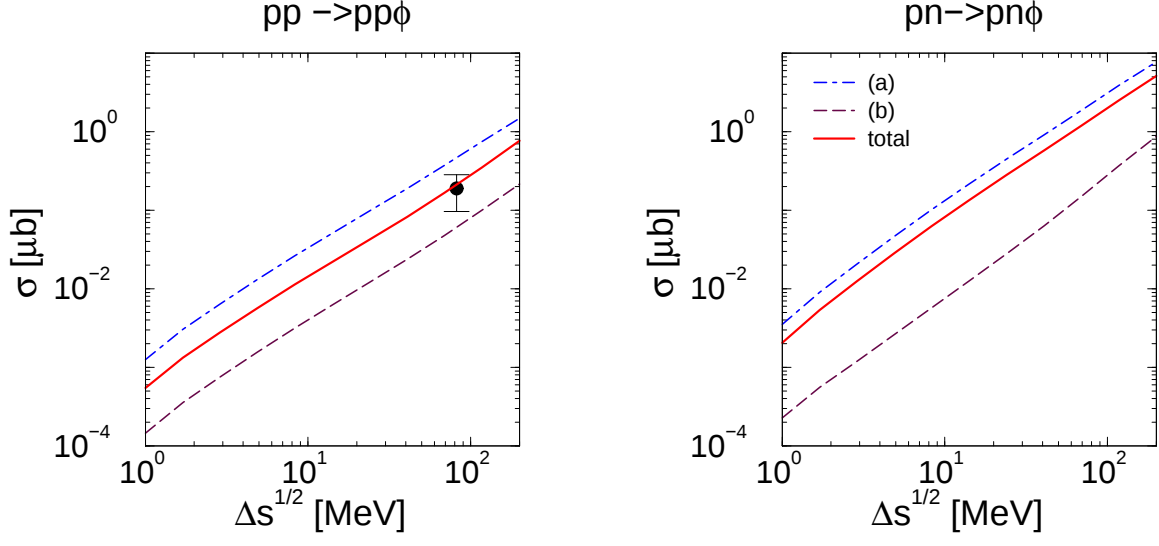
FIG. 13.　The same as in Fig. 12, but for the parameter set C.
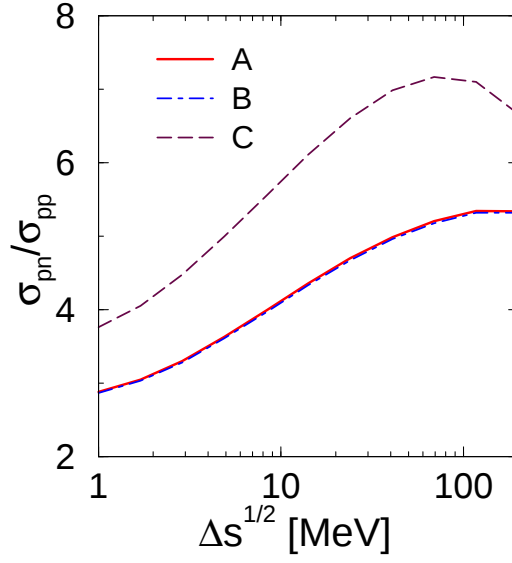


FIG. 14.　The energy dependence of the ratio of the total cross sections of $pp \rightarrow pp\phi$ and $pn \rightarrow pn\phi$ reactions for different parameter sets.
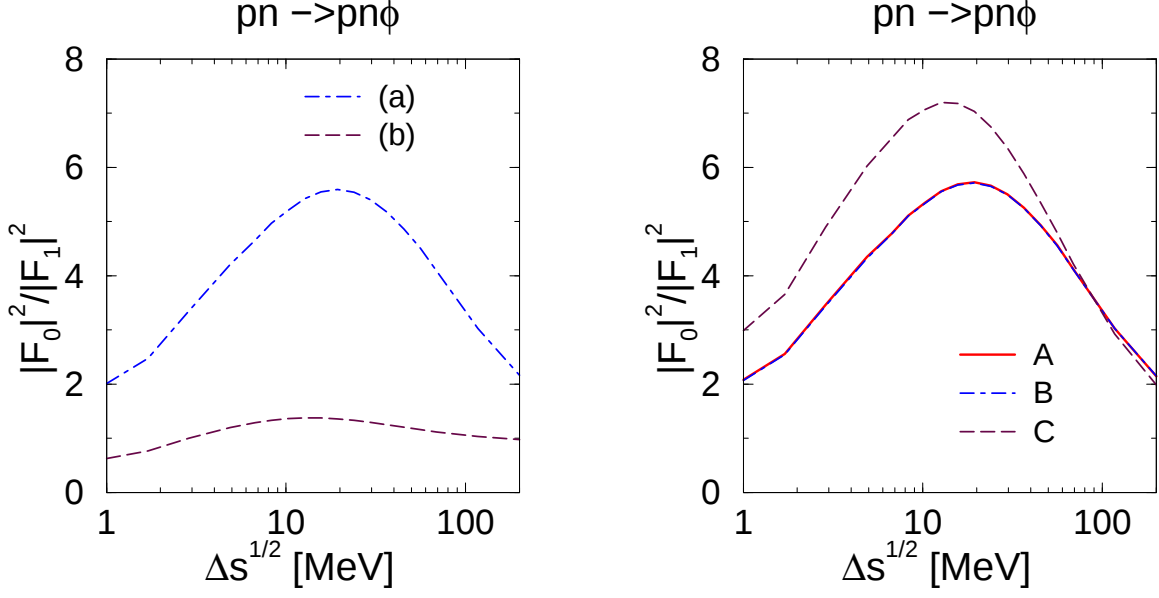
FIG. 15.    The energy dependence of the ratio of the initial singlet to triplet cross sections in *pn* interaction for separate channels (left panel) and for different parameter sets (right panel).
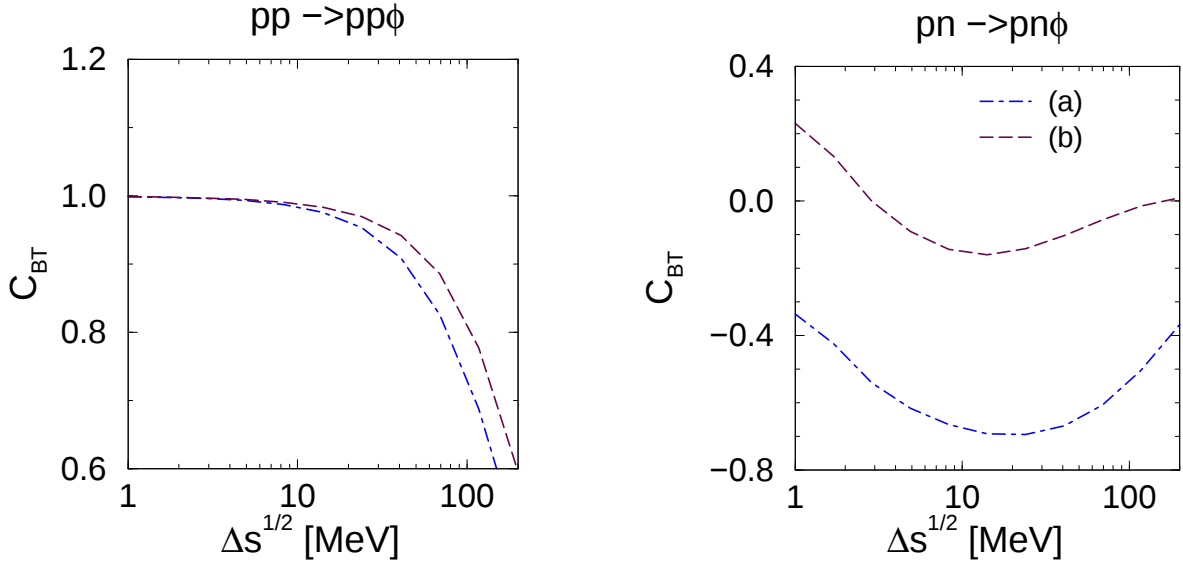


FIG. 16.    The beam target asymmetry for separate channels for *pp* (left panel) and *pn* (right panel) interactions.
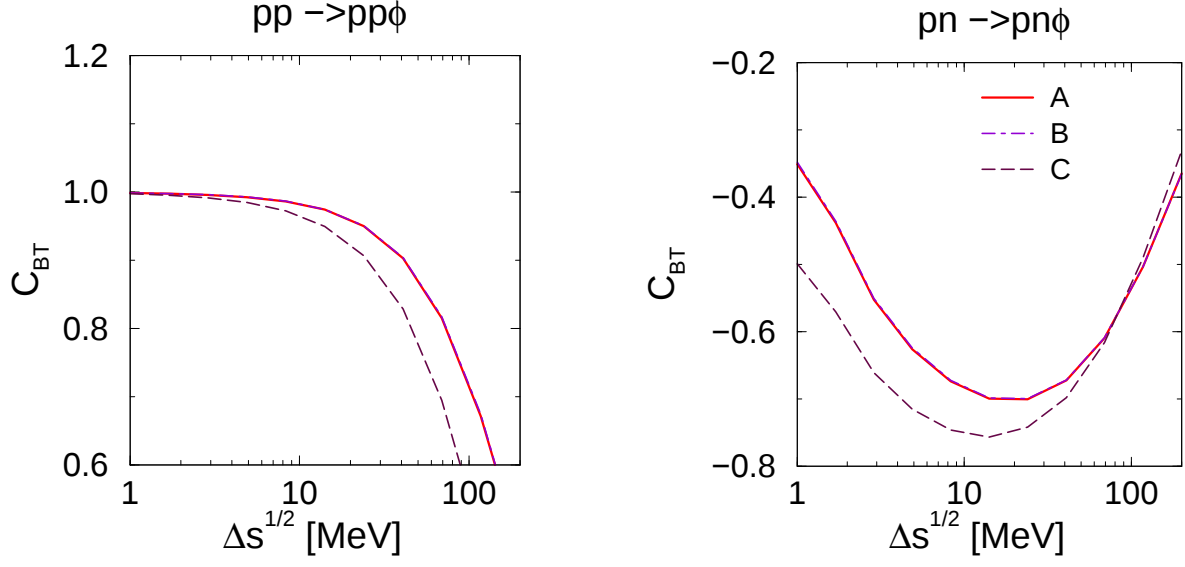
FIG. 17.   The same as in Fig. 15 but for different parameters sets.
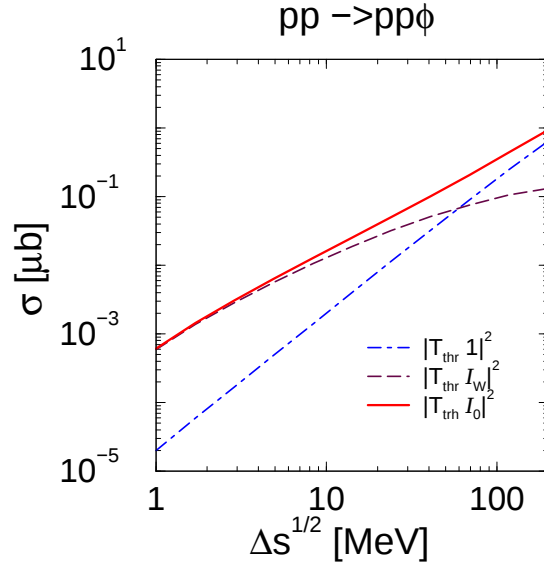


FIG. 18.   The effect of FSI for different enhancement factors for the parameter set B in the reaction $pp \rightarrow pp\phi$. Notation is explained in the text.